R3-A.3: Multi-Transmitter/Multi-Receiver Blade Beam Torus Reflector for Efficient Advanced Imaging Technology

I. PARTICIPANTS INVOLVED FROM JULY 1, 2019 TO JUNE 30, 2020

Faculty/Staff			
Name	**Title**	**Institution**	**Email**
Carey Rappaport	PI	NEU	c.rappaport@northeastern.edu
Jose Martinez	Faculty	NEU	j.martinez-lorenzo@northeastern.edu
Dan Busuioc	Consultant	DBC Group, Inc.	db.ipaq@gmail.com
Graduate, Undergraduate and REU Students			
Name	**Degree Pursued**	**Institution**	**Month/Year of Graduation**
Mohammad Nemati	PhD	NEU	TBD
Mahshid Asri	MS, PhD	NEU	5/2020 (MS), 5/2023 (PhD)
Muhammad Ghafoor	BS	NEU	5/2021
Maulik Patel	BS	NEU	5/2025
Emily Belk	BS	NEU	5/2023
Thomas Campion	BS	NEU	5/2022

II. PROJECT DESCRIPTION

A. Project Overview

We have developed a custom-designed advanced imaging technology (AIT) person-scanning system that represents the next generation of airport and other secure-area concealed object detectors. The currently employed systems are omnipresent in the United States and worldwide [1-4]. Our system uses an elliptical toroid reflector that allows multiple overlapping beams for focused wide-angle illumination to speed data acquisition and accurately image strongly inclined body surfaces. Building on the concepts and analysis of ALERT's project R3-A.1 [5-7], we have extended the blade beam reflector from a single illuminating antenna into a multibeam toroidal reflector, with multiple feeds. Each feed generates a different incident beam with different viewing angles, while still maintaining the blade beam configuration of narrow slit illumination in the vertical direction. Having multiple transmitters provides horizontal resolution and imaging of a full 110 degrees of body. Furthermore, the reflector can simultaneously be used for receiving the scattered field, with high-gain, overlapping, high-vertical-resolution beams for each transmitting or receiving array element. The multistatic transmitting and receiving array configuration sensing avoids dihedral artifacts from body crevices and reduces nonspecular dropouts [8, 9].

We have extended the toroidal-reflector–based system from a single fixed transmitter (Tx), swinging arc receiver (Rx) design, to a fixed array of seven transmitters with overlapping coverage (Figure 1). We have computationally simulated, designed, and fabricated radar modules; designed mounts; built a radio frequency (RF) switching network; and assembled and tested a fifty-receiver/seven-transmitter fixed array.

The designs for the fixed array of receivers and transmitters are shown in Figure 1. This configuration was the result of many man-hours of work: (i) we minimized the spacing while maintaining the appropriate distance between elements to mimic the performance of an array with about a third as many elements as previous studies; (ii) we positioned transmitters to block receivers minimally, keeping the antenna elements close enough to the mathematically ideal focal arc while allowing for assembly and fine-tuning for real-world optimal repositioning; (iii) we supported the radar module boards in high temperature conditions to ensure that the multistatic signals are received strongly for all target positions from -55 to 55 degrees, and (iv) we designed to allow for heat-sink attachments. We have simplified the cabling and positioning infrastructure for easy and fast channel assignment.

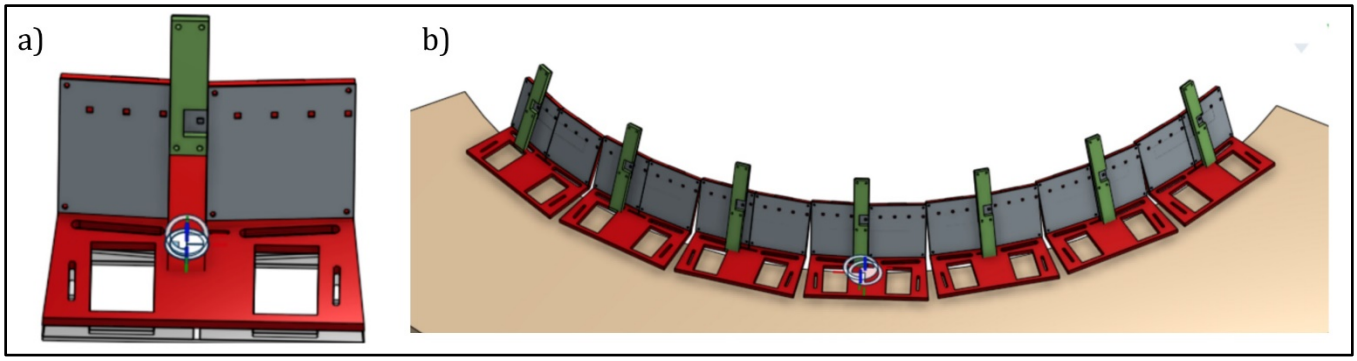

Figure 1: SolidWorks designs of (a) the front view of an individual mount with (green) an attached transmitter board and (gray) two quad receiver boards, showing (small red squares) antenna element positions; and (b) the full seven-mount, fifty-six–receiver array.

B. State of the Art and Technical Approach

The toroidal reflector antenna images in the horizontal plane and translates vertically. As such it acquires signals faster and is prone to fewer mechanical alignment, ruggedness, and wear operation issues than 2D raster scan systems [10]. The toroidal shape can be thought of as a surface of revolution, in which an elliptical profile is swept from -55 to 55 degrees in a 1.06 m circular arc about a vertical axis. The circular horizontal profile is well-approximated by infinitely many parabolas, each with focal length roughly half the circle radius and focal point on a concentric circular arc also having a radius of one half the circle radius. These approximate parabolic contours each act to collimate reflected horizontal rays, while the elliptical vertical contour focuses rays to the secondary focal point in a vertical plane. The resulting reflector reflects rays from any feed point on the focal arc into a "blade beam" that focuses to a line passing through the secondary ellipse focal point. Because of the circular symmetry of the toroidal reflector, there are infinitely many portions that produce blade beams, each inclined in horizontal azimuth. We choose seven equi-angular points on the focal arc for transmitter points, and fifty positions on the arc as receiver positions, as shown in Figure 1. The elliptical contours are chosen as offset to the major ellipse axis to ensure the feeding antenna elements do not block reflected rays. This accounts for the antenna mounts being tilted backwards, which causes each element main beam to be directed upward.

The overall reflector configuration requires precision mounting but can in principle capture the entire front or back horizontal body cross-section practically simultaneously, with 7 × 50 channels (78% more than currently employed systems). In addition, the multistatic configuration avoids dihedral artifacts from body crevices and shadowing drop-outs. The signal processing is also more efficient—and motion artifacts can be reduced, since each horizontal cross-section contour can be computed separately, as soon as it is measured, instead of waiting to have all measurements at all antenna positions taken first.

C. Major Contributions

- Development of an elliptical torus reflector for overlapping multibeam transmission and reception for multistatic operation (2013).
- Fabrication of a reflector and experimental proof of principle (2014).
- Multistatic imaging with elliptical torus using an original Tx/Rx chipset (2015).
- Design of 60-GHz multistatic radar Tx and Rx modules, including separated motherboard/daughterboard configuration, as demanded by the manufacturer's revised specification (2016).
- Design of a separated 60-GHz wideband microstrip antenna (2017).
- Fabrication and testing of RF single Tx/Rx boards (2018).
- Debugging and imaging using individual RF Tx/Rx boards (2019).
- Design and fabrication of quad Rx motherboard and daughterboard to minimize packaging and cabling (2019).
- Correction of a subtle design flaw and second fabrication (2019).
- Debugging of twenty-seven fabrication-delayed quad receiver and transmitter boards (2020).
- Self-calibration protocol, hardware configuration and algorithm to compensate for random receiver and transmitter 180-degree phase errors (2020).
- Thermal compensation of entire test setup (2020).
- Development, testing, and implementation, of position compensation post-processing algorithm to refocus misaligned receiver array elements (2020).

D. Milestones

- Due to the COVID-19–related delays described in the next section, along with the abrupt cancellation of funding by Smiths following their reorganization, almost none of the major milestones originally established were attained. The automatic full 3D reconstruction of a mannequin body surrogate is still to be realized, and the implementation of the dual frequency imaging scheme has not been demonstrated.
- One important goal that was achieved was the demonstration that a fixed array of receivers and transmitters can operate faster than a rotating single receiver. This was a major deliverable at the outset of R3-A.3. Although 3D imaging is still being pursued, the unexpectedly challenging issues of hardware positioning and mounting were solved (Figure 2), as was the thorny issue of calibrating the receivers' starting signal values. This latter difficulty was another flaw in the chip design that resulted in random 180 phase variations. These were overcome by installing a pair of reference transmitters and receivers to correct for the sign flip whenever it occurred.
- New chips by sole source vendor ADI have been pursued to mitigate the random phase effects and significantly increase the operating bandwidth. But this also has been delayed indefinitely by the manufacturer due to performance failures and the COVID-19 shutdown.
- Another midcourse hardware mitigation strategy that was put into place was developing an algorithm to compensate for inaccurate installation of the extremely sensitive positioning. This is discussed in detail in the next section.

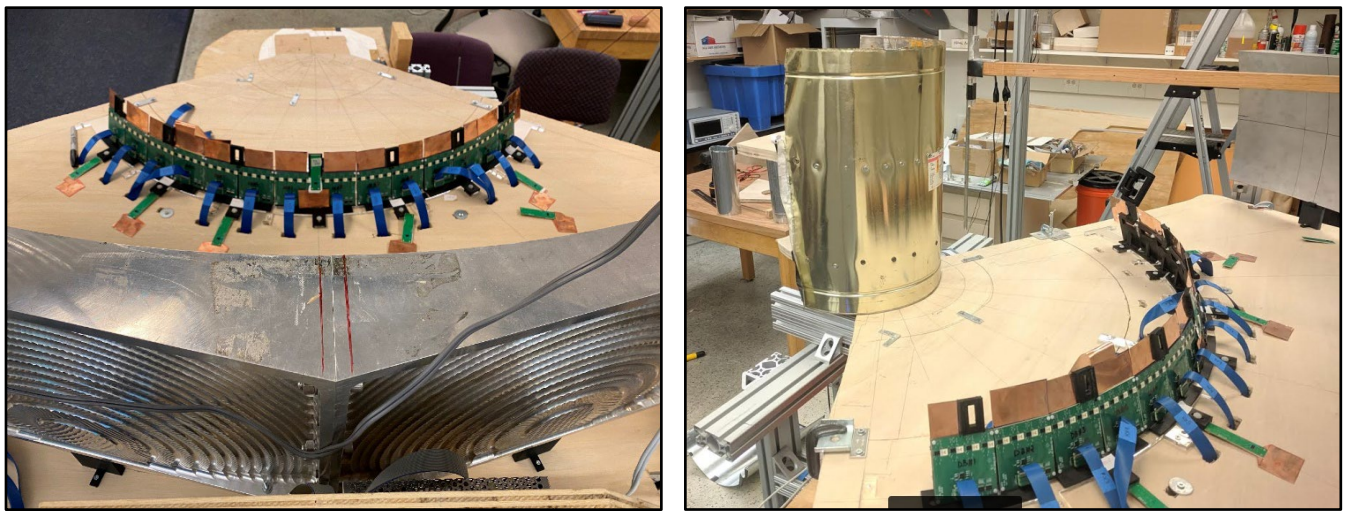

Figure 2: Two views of the fifty-six–element receiver and seven-element transmitter arrays, co-located on a circular arc and tilted to face the center plane of the elliptical torus reflector. The receivers (small grey squares) are mounted four to a board, and the transmitters are singly mounted on narrow green boards. The positions have been extensively analyzed, simulated, and optimized to measure the greatest amount of information in the limited space available.

E. Final Results at Project Completion (Year 7)

The progress on R3-A.3 has been disappointing in Year 7 because of four factors, two of which are due to COVID-19: (i) The custom fabrication of the radar modules was originally contracted to a firm in China in January, just as the country shut down in response to the novel coronavirus outbreak. After two months of uncertain delivery, we shifted the fabrication to a firm in New Hampshire, only to suffer the same stop-work, as COVID-19 and its lockdown reached the United States. The circuit boards were finally delivered, but Northeastern University (NU) shut down soon afterward. All told, the fabrication delay resulted in about three months of lost project time. (ii) Perhaps as a result of the reduced capacity of the fabricator, the quality of the circuit boards was inconsistent. The sole student who was permitted in the NU AIT lab had to painstakingly trace each of fourteen receiver boards and seven transmitter boards, debugging—and occasionally repairing—errors in the delivered hardware. In addition, it became apparent that the chips were generating excessive heat and needed extreme cooling measures. Heat sinks and cooling fans were designed, but high-power fans were required to keep the chip temperature within tolerance (Figure 3). After an additional two and a half months, the RF electronics were finally made operational within the expected performance parameters. (iii) The positions of the installed receivers and transmitters were found to be inexact, and the sensitive imaging results became totally garbled. Since the center wavelength of the radar system is 5 mm, a positioning error of just 2.5 mm would cause a phase error of 180 degrees, or 100% error. Despite great care in fabrication, this installation position error dominated the imaging (Figure 4). We found ways to compensate for it and refocus in postprocessing, but this also took time to develop. (iv) The graduate student, Mohmmad Nemati, who had been running the experimental facility since its inception, accepted full-time employment in May and left for California without completing his dissertation. Replacing him at this last date is problematic.

Figure 3: Elliptical reflector antenna with transmitters and receivers (orange) cooled by large fans. A metallic air duct cylinder body part surrogate target is positioned in the target region.

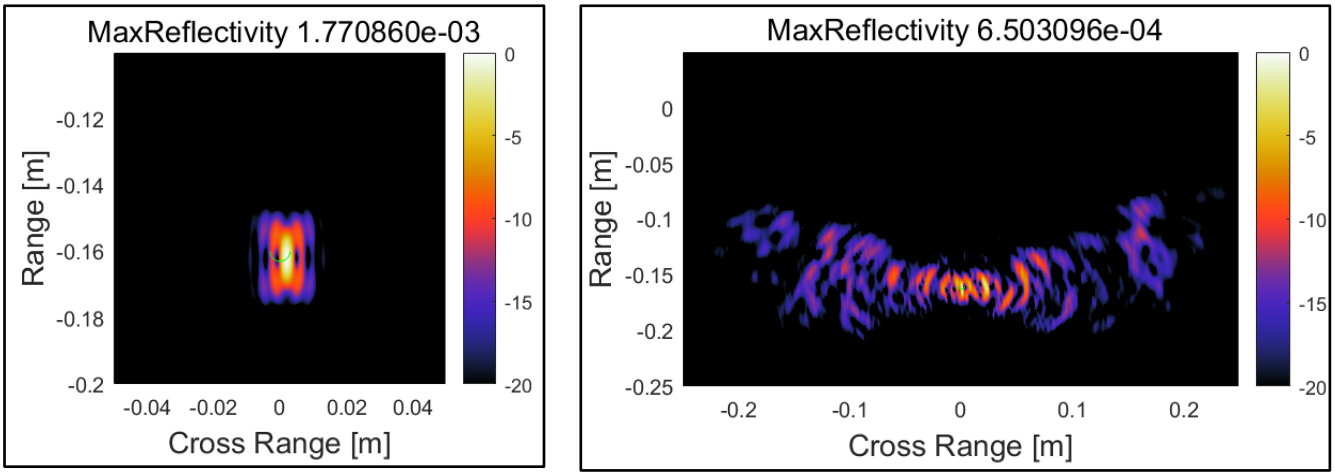

Figure 4: (a) Expected reconstructed image of a simulated thin vertical pole in cross section, producing a tight spot at the correct target position; (b) reconstructed image from experimentally measured radar data from inaccurately aligned receivers.

The most important contribution in R3-A.3 is the position compensation algorithm. This postprocessing algorithm corrects for the slight but extremely sensitive position errors in the hardware installation. Errors too small to measure mechanically cause significant defocusing and destroy the imaging. The example of reconstructing a de facto point scatterer is shown for a modeled case in Figure 4. For reconstruction of large structures, the imaging system must first accurately image the smallest point source objects. The image in Figure 4b clearly indicates the poor, unfocused image of a small localized scatterer. The problem comes from the excess path length between the installed receiver position and the ideal position that is assumed for the imaging algorithm.

The algorithm developed to compensate for the installation position error is simple in principle but challenging to implement. The first step is to determine the phase errors corresponding to the position error for the n^{th} receiver, relative to all the receivers. This can be done by observing the phase at the presumed location of the calibration poles. The difference between the expected phase and the observed phase for the n^{th} receiver, $\Delta\Phi_n$, is a measure of the defocusing. Graphically, this is seen as choosing the shortest distance from each straight receiver signal line in Figure 5b to the pole position (0, -0.15). Since the position error has two components, the phase difference for each receiver must be found for two calibration poles $\Delta\Phi_{n\binom{1}{2}}$.

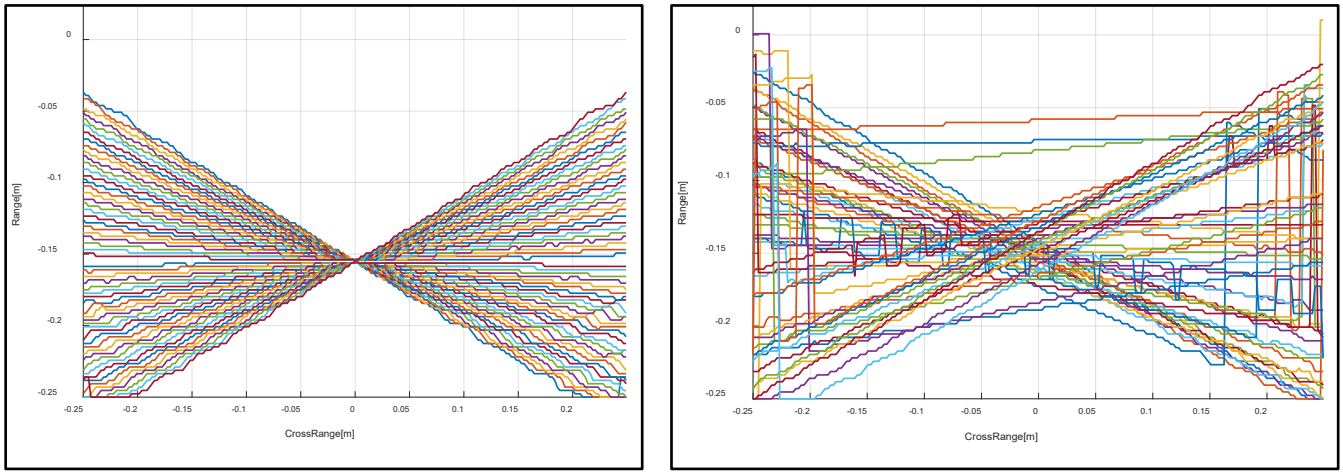

Figure 5: 1D inversions for each of fifty-six receivers separately (different color lines) when the scatterer is a thin metal pole located at (0, -0.15); (a) modeled inversion with no installed position error, indicating that all receivers constructively interfere only at the point target location and destructively interfere at other range and cross-range positions. The 1D images are straight lines for our particular antenna geometry, in which the reflector generates parallel (or plane wave) incident and received rays; (b) 1D inversions based on experimentally measured data using the AIT elliptical torus reflector, indicating five large excursions due to random 180-degree phase errors and many other errors due to inaccurately aligned receivers.

Next, the path length is found for rays traced from the n^{th} installed receiver back through the reflector along the collimated plane-wave rays in the midplane of the reflector to the target calibration pole position. In terms of the ideal receiver position, the installed position of the n^{th} receiver is $(\delta r_i, \theta_i) = \left(r_p - f_r\,, \theta_{n0}\right) + (\delta r_n, \delta\theta_n)$, where f is the offset parabolic reflector midplane section focal length, f_r is the radial component of the focal vector, and r_p is the radius of the torus. The last term is the positioning error, or distance that must be compensated for the n^{th} receiver. Phase is related to distance by $\Phi_n = -k\, r_n$. Assuming the position errors are small relative to the focal length, an effective linearization for each pole results in the phase difference as a simple function of perturbed distances for the n^{th} receiver:

$$\Delta\Phi_{n\binom{1}{2}} = k\left(\frac{f_r}{f}\,\delta r_n + y_{n\binom{1}{2}}\left(\frac{r_p}{f_r} - 1\right)\,\delta\theta_n\right)$$

where

$$y_{n\binom{1}{2}} = r_{\binom{1}{2}}\sin\left(\theta_{\binom{1}{2}} - \theta_{n0}\right)$$

Solving the pair of simultaneous linear equations (one for each pole), the error for the n^{th} receiver is then given by:

$$(\delta r_n, \delta\theta_n) = \left(\frac{f}{kf_r} \frac{y_{n1}\Delta\Phi_{n2} - y_2\Delta\Phi_{n1}}{y_{n1} - y_{n2}}, \qquad \frac{f_r(\Delta\Phi_{n1} - \Delta\Phi_{n2})}{k(f_r - r_p)(y_{n1} - y_{n2})} \right)$$

where r_1 and r_2 are the distances from the center of rotation of the torus to the n^{th} receiver and the first and second thin calibration poles, and θ_{n0}, θ_1, and θ_2 are the angles from the axis of symmetry to the n^{th} receiver and the first pole and the second pole, respectively. Once the position errors have been found, a phase difference correction $\Delta\Phi_{nm}$ for the n^{th} receiver at any image point at (r_m, θ_m) can be found using the first formula with $y_{n\binom{1}{2}}$ replaced with y_{nm}.

Only the receiver positions have been compensated for in the above development. The transmitter positions are also subject to alignment issues, but since they lie on the same focal arc as receivers, the same approach applies to compensate for their position errors.

An example of the effectiveness and precision of the algorithm is demonstrated for a modeled case where the receivers are randomly displaced in radial and angular directions. Thin metal poles at (*x*, *y*) = (-0.02, -0.14) and (0.035, -0.120) (positions are in meters relative to the axis of rotation of the toroidal reflector) are used as the calibration targets. Figure 6 shows the before-and-after compensation pairs of images for nine target position cases (three-by-three grid) in the images space. For each of the nine positions, the left image (before compensation) is smeared and unfocused with little information about where the target should be, while the right image (after compensation) looks almost exactly like the PSF of the point scatterer at the proper position.

Note that this method is much more efficient than reinverting the imaging equations using the derived installed receiver positions because it combines images—each weighted pixel by pixel—instead of recomputing the scattering matrix.

The next step is to apply the postprocessing position error compensation algorithm to collections of point targets, including large body-part surfaces. This will be our approach going forward.

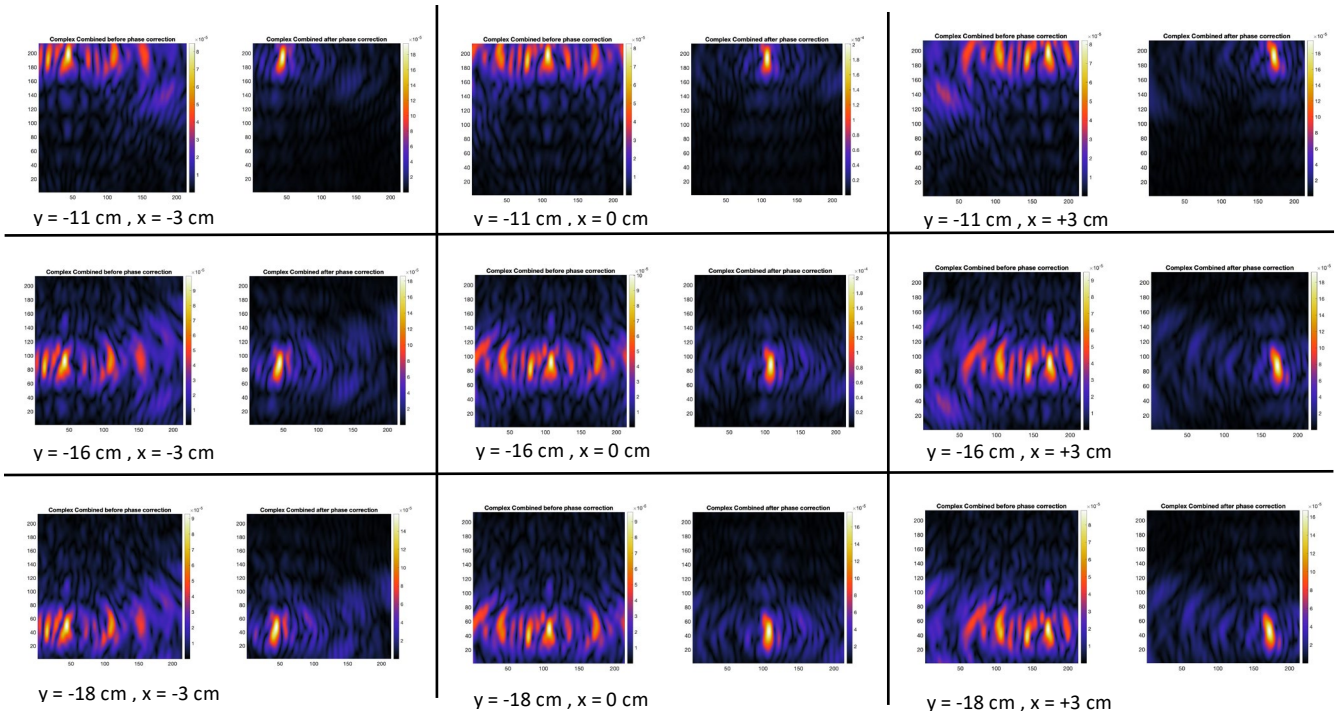

Figure 6: Simulated imaging of a single thin metal pole at nine locations, (left of each pair) without and (right of each pair) with receiver position compensation postprocessing. Receivers have independent random installation errors in both radial and circumferential directions, not exceeding half wavelength (±2.5 mm). These errors defocus the reconstructed image, resulting in smearing and disorganization, while the compensated processed image is crisp, tight, and positioned exactly at each of the various pole positions.

III. RELEVANCE AND TRANSITION

A. Relevance of Research to the DHS Enterprise

- **Relevance #1:** Faster, artifact-free, multistatic (shadow-free) imaging has been important to AIT since TSA's inception. R3-A.3 provides experimental proof that revolutionary improvements are attainable within the constraints of the current concept of operation. By eliminating the shadowing inherent in multimonostatic or bistatic radar, the images of the inside portion of each leg and arm will not suffer from gaps of missing data in the reconstruction. More work is needed to fully demonstrate the reflector-based nearfield imaging radar, but the basic concept is sound.
- **Relevance #2:** The cost for our multistatic design has been shown to be lower than the currently fielded systems. This is due to commercial off-the-shelf 60-GHz radio receiver and transmitter chips that have been repurposed as radar modules. The cost for each module is less than $100, so a seven-transmitter, fifty-receiver multistatic radar would cost about $17 per channel. The processing requires analog-to-digital converters and computer CPU processors, but these costs are low for volume purchasing.
- **Relevance #3:** As R3-A.3 has been developed in conjunction with the algorithm development project R3-A.2, it is automatically well suited for incorporating material characterization. The multistatic reflector-based nearfield radar automatically measures the thickness of foreign objects on the body and can be used to determine the dielectric constant of weak dielectric slabs. This is particularly relevant as a means of ruling out innocent objects, such as cash in a money belt, while alarming on explosive slabs.

B. Transition at Project End

Because of the management realignment and the reprioritization of research and development work at our primary partner, Smiths Detection, our major deliverable in R3-A.3 was cancelled. As such, our plans for transition have not been successful. There is still interest in the experimental AIT project, but commitment of funds is not forthcoming.

C. Transition Pathway and Future Opportunities

We continue to explore improvements in AIT design with both Smiths Detection and Rapiscan, despite scientific staff changes at each organization. Our main proponent at Smiths was laid off due to business activity reduction during the COVID-19 shutdown. We are considering joint proposals to DHS, including the current DHS BAA (HSHQDC-16-R-B0004).

D. Customer Connections

- Christopher Gregory, Smiths Detection, monthly calls
- Dan Strellis, Rapiscan, quarterly calls, occasional email

IV. PROJECT ACCOMPLISHMENTS AND DOCUMENTATION

A. Education and Workforce Development Activities

1. Student Internship, Job, and/or Research Opportunities
    a. Mohammad Nemati is completing his doctorate with a dissertation based on this project.
    b. Guanying Sun is pursuing research for her dissertation using data from this project.
    c. Mahshid Asri completed her master's thesis using data from this project.
    d. Muhammad Ghafoor, Christos Tsevis, Maulik Patel, Thomas Campion, and Emily Belk have been volunteer undergraduate researchers working on this project.

B. Peer Reviewed Conference Proceedings

1. Tajdini, M., & Rappaport, C. "Focused CW Mm-Wave Characterization of Lossy Penetrable Dielectric Slab Affixed to Human Body." *2019 IEEE International Symposium on Antennas and Propagation*, Atlanta, GA, July 2019.
2. Asri, M., & Rappaport, C. "Automatic Permittivity Characterization of a Weak Dielectric Attached to Human Body Based on Using Wideband Radar Image Processing." *2019 IEEE International Symposium on Antennas and Propagation*, Atlanta, GA, July 2019.
3. Morgenthaler, A., & Rappaport, C. "Modeling Focused CW Mm-Wave Scattering of a Penetrable Dielectric Slab Affixed to a Human Body." *2019 IEEE International Symposium on Antennas and Propagation*, Atlanta, GA, July 2019.
4. Sun, G., Nemati, M., & Rappaport, C. "Improving the Reconstruction Image Quality of Multiple Small Discrete Targets Using the Phase Coherence Method." *European Conference on Antennas and Propagation*, Copenhagen, Denmark, March 2020.

C. Other Presentations

1. Rappaport, C. "Multistatic 3D Whole Body Millimeter-Wave Imaging for Explosives Detection." *IEEE Distinguished Lecture*, Qualcomm, San Diego, CA, 6 December 2019.
2. Rappaport, C. "Multistatic 3D Whole Body Millimeter-Wave Imaging for Explosives Detection." *IEEE Distinguished Lecturer* speech, University of Lund, Lund, Sweden, 5 March 2019.

D. Student Theses or Dissertations Produced from This Project

1. Asri, M. "Automatic Characterization of Low-Loss Low-Permittivity Body-Born Threats Using Wideband Millimeter-Wave Radar." MS Thesis, ECE, Northeastern University, April 2020.

E. Technology Transfer/Patents

1. Patents Awarded
   a. Martinez Lorenzo, J., & Rappaport, C. "Characterization of Dielectric Slabs Attached to the Body Using Focused Millimeter Waves." #10,416,094, 17 September 2019.

Year 6 Patent Not Previously Reported –

a. Gonzales Valdes, B., Martinez Lorenzo, J., & Rappaport, C. "On the Move Millimeter Wave Interrogation System with a Hallway of Multiple Transmitters and Receivers." # 10,295,664, 21 May 2019.

V. REFERENCES

[1] J. Skorupski and P. Uchronski, "Evaluation of the effectiveness of an airport passenger and baggage security screening system," *Journal of Air Transport Management*, vol. 66, pp. 53–64, 2018.

[2] R. Sakano, K. Obeng, and K. Fuller, "Airport security and screening satisfaction: A case study of us," *Journal of Air Transport Management*, vol. 55, pp. 129–138, 2016.

[3] A. Knol, A. Sharpanskykh, and S. Janssen, "Analyzing airport security checkpoint performance using cognitive agent models," *Journal of Air Transport Management*, vol. 75, pp. 39–50, 2019.

[4] A. Pala and J. Zhuang, "Security screening queues with impatient applicants: A new model with a case study," *European Journal of Operational Research*, vol. 265, no. 3, pp. 919–930, 2018.

[5] Rappaport, C.M., and Gonzalez-Valdes, B., "The blade beam reflector antenna for stacked nearfield millimeter-wave imaging," *IEEE Antennas and Propagation Society Int'l Symp.*, pp.1-2, 8-14 July 2012.

[6] Gonzalez-Valdes, B., Y. Alvarez, J. A. Martinez-Lorenzo, F. Las-Heras, and C. M. Rappaport, "On the Use of Improved Imaging Techniques for the Development of a Multistatic Three-Dimensional Millimeter-Wave Portal for Personnel Screening," *Progress In Electromagnetics Research, PIER*, vol. 138, pp. 83-98, 2013.

[7] Alvarez, Y., Gonzalez-Valdes, B., Martinez-Lorenzo, J., Las-Heras, F., and Rappaport, C.M., "3D Whole Body Imaging for Detecting Explosive-Related Threats," *IEEE T. Antennas and Propagation*, vol. 60, no. 9, pp. 4453,4458, Sept. 2012.

[8] D. M. Sheen, D. L., McMakin, and T. E. Hall, "Combined illumination cylindrical millimeter-wave imaging technique for concealed weapon detection," *AeroSense, International Society for Optics and Photonics*, pp. 52-60, July 2000.

[9] D. M. Sheen, D. L. McMakin, and T. E. Hall, “Three-dimensional millimeter-wave imaging for concealed weapon detection,” *IEEE Transactions on Microwave Theory and Techniques*, vol. 49, no. 9, pp. 1581–1592, 2001.

[10] Cooper, K.B., Dengler, R.J., Llombart, N., Thomas, B., Chattopadhyay, G., and Siegel, P.H., "THz Imaging Radar for Standoff Personnel Screening," *IEEE T. Terahertz Science and Technology*, , vol. 1, no. 1, pp.169-182, Sept. 2011.